2022

Mitochondrial redox environments predict sensorimotor brain-behavior dynamics in adults with HIV.

Rachel K. Spooner

Brittany K. Taylor

Iman M. Ahmad

Kelsey Dyball

Katy Emanuel

See next page for additional authors

Authors

Rachel K. Spooner, Brittany K. Taylor, Iman M. Ahmad, Kelsey Dyball, Katy Emanuel, Jennifer O'Neill, Maureen Kubat, Susan Swindells, Howard S. Fox, Sara Bares, Kelly L. Stauch, Matthew C. Zimmerman, and Tony W. Wilson

Brain, Behavior, and Immunity 107 (2023) 265–275

Contents lists available at ScienceDirect

Brain Behavior and Immunity

journal homepage: www.elsevier.com/locate/ybrbi

Full-length Article

Mitochondrial redox environments predict sensorimotor brain-behavior dynamics in adults with HIV

Rachel K. Spooner [a,b,c,*], Brittany K. Taylor [a,d], Iman M. Ahmad [e], Kelsey Dyball [f], Katy Emanuel [f], Jennifer O'Neill [g], Maureen Kubat [g], Susan Swindells [g], Howard S. Fox [f], Sara H. Bares [g], Kelly L. Stauch [f], Matthew C. Zimmerman [h], Tony W. Wilson [a,b,d]

[a] Institute for Human Neuroscience, Boys Town National Research Hospital, Boys Town, NE, USA
[b] College of Medicine, University of Nebraska Medical Center (UNMC), Omaha, NE, USA
[c] Institute of Clinical Neuroscience and Medical Psychology, Heinrich-Heine University, Düsseldorf, Germany
[d] Department of Pharmacology and Neuroscience, Creighton University, Omaha, NE, USA
[e] College of Allied Health Professions, UNMC, Omaha, NE, USA
[f] Department of Neurological Sciences, UNMC, Omaha, NE, USA
[g] Department of Internal Medicine, Division of Infectious Diseases, UNMC, Omaha, NE, USA
[h] Department of Cellular and Integrative Physiology, UNMC, Omaha, NE, USA

ARTICLE INFO

Keywords:
Magnetoencephalography
Neural oscillations
Motor cortex
EPR spectroscopy
Seahorse analyzer
Superoxide
Hydrogen peroxide

ABSTRACT

Despite virologic suppression, people living with HIV (PLWH) remain at risk for developing cognitive impairment, with aberrations in motor control being a predominant symptom leading to functional dependencies in later life. While the neuroanatomical bases of motor dysfunction have recently been illuminated, the underlying molecular processes remain poorly understood. Herein, we evaluate the predictive capacity of the mitochondrial redox environment on sensorimotor brain-behavior dynamics in 40 virally-suppressed PLWH and 40 demographically-matched controls using structural equation modeling. We used state-of-the-art approaches, including Seahorse Analyzer of mitochondrial function, electron paramagnetic resonance spectroscopy to measure superoxide levels, antioxidant activity assays and dynamic magnetoencephalographic imaging to quantify sensorimotor oscillatory dynamics. We observed differential modulation of sensorimotor brain-behavior relationships by superoxide and hydrogen peroxide-sensitive features of the redox environment in PLWH, while only superoxide-sensitive features were related to optimal oscillatory response profiles and better motor performance in controls. Moreover, these divergent pathways may be attributable to immediate, separable mechanisms of action within the redox environment seen in PLWH, as evidenced by mediation analyses. These findings suggest that mitochondrial redox parameters are important modulators of healthy and pathological oscillations in motor systems and behavior, serving as potential targets for remedying HIV-related cognitive-motor dysfunction in the future.

1. Introduction

HIV infection is associated with a host of comorbidities, including cognitive and behavioral dysfunction that persists despite effective combination antiretroviral therapy (cART) (Antinori et al., 2007; Cysique and Brew, 2009; Heaton et al., 2011, Heaton, 2010; Kamkwalala and Newhouse, 2017; Robertson et al., 2007; Saylor et al., 2016; Simioni et al., 2010). Interestingly, one of the first behavioral abnormalities that manifests in those with HIV-related cognitive impairment is that of motor dysfunction (Cysique and Brew, 2009; Elicer et al., 2018; Robinson-Papp et al., 2020; Valcour et al., 2008; Wilkins et al., n.d.). In fact, the original terminology for characterizing mild to moderate forms of HIV-associated neurocognitive disorder (HAND) included a condition termed HIV-associated mild cognitive-motor disorder (MCMD) (Ances and Clifford, 2008; "Nomenclature and research case definitions for neurologic manifestations of human immunodeficiency virus-type 1 (HIV-1) infection. Report of a Working Group of the American Academy of Neurology AIDS Task Force," 1991). While previous investigations

* Corresponding author at: Heinrich-Heine University Düsseldorf, Universitätsstraße 1, 40225 Düsseldorf, Germany.
E-mail address: rachelkae.spooner@med.uni-duesseldorf.de (R.K. Spooner).

https://doi.org/10.1016/j.bbi.2022.10.004
Received 12 April 2022; Received in revised form 23 August 2022; Accepted 9 October 2022
Available online 19 October 2022

have made major progress in characterizing the structural and functional aberrations that occur within the sensorimotor cortical and subcortical networks in people living with HIV (PLWH) (Becker et al., 2011; Cohen et al., 2010; Thompson et al., 2005; Wang et al., 2011; Zhou et al., 2017), far less is known about the underlying neuronal dynamics and key molecular pathways that govern such marked declines in motor function. This is unfortunate, as HIV-related deficits in motor control may play an important role in the non-motor symptoms that persist in the modern cART era and further, these impairments profoundly impact a person's functional dependence in later life.

In regard to circuitry, motor control requires a coordinated ensemble of spatiotemporally-precise neural oscillations during the planning, execution and termination phases of movement. Recent neurophysiological studies have primarily focused on movement-related oscillations in the beta range (i.e., 15–30 Hz), which exhibit robust decreases in power prior to and following movement onset across an extended motor network including bilateral primary motor cortices (M1), supplementary motor areas (SMA), and parietal cortices (Grent-'t-Jong et al., 2014; Heinrichs-Graham et al., 2016; Tzagarakis et al., 2010; Wilson et al., 2014). Importantly, this distinct pattern of oscillatory activity is thought to reflect the active engagement of neuronal pools and further, is sensitive to higher-order cognitive demands of the action to be performed (e.g., response certainty (Grent-'t-Jong et al., 2014; Heinrichs-Graham et al., 2016; Kaiser et al., 2001; Praamstra et al., 2009; Tzagarakis et al., 2010), complexity (Heinrichs-Graham and Wilson, 2015), interference (Grent-'t-Jong et al., 2013; Heinrichs-Graham et al., 2018a; Heinrichs-Graham et al., 2018b; Spooner et al., 2021a; Wiesman et al., 2020)), making its role in behavioral modification particularly important. To date, only one prior study has evaluated the impact of HIV on beta oscillations during movement. In 2013, Wilson et al. used a simple finger tapping paradigm during magnetoencephalography (MEG) and observed a strong attenuation of peri-movement beta power (i.e., −350 to 250 ms surrounding movement onset) in the bilateral M1 and the SMA in PLWH compared to uninfected controls (Wilson et al., 2013). In contrast, PLWH exhibited stronger beta responses during movement onset in prefrontal regions (Wilson et al., 2013), which aligns well with prior functional magnetic resonance imaging (fMRI) literature demonstrating hypoactivity in primary sensory regions (Ances et al., 2011, Ances et al., 2010, Ances et al., 2009) and hyperactivity in association cortices that govern task performance in PLWH (Chang et al., 2008, 2004; Ernst et al., 2009, Ernst et al., 2002). Importantly, while this study provided novel insight regarding aberrant peri-movement beta oscillatory responses in PLWH, it did not attempt to link these oscillatory dynamics to behavioral performance. Regardless, more complex motor tasks would be better equipped to elicit behavioral differences that could be quantified in real time alongside neuromagnetic recordings.

Underlying the neural oscillatory profiles that govern motor function are the molecular mechanisms that are broadly seen as potential contributors to the age- and disease-related decline in brain-behavior dynamics. One such mechanism involves a mitochondrial-induced redox imbalance of the system, which suggests that mitochondrial dysfunction (e.g., deficient oxygen consumption) leads to an accumulation of reactive oxygen species (ROS), concomitant with an attenuation of their antioxidant defenses, leading to a host of comorbidities observed in aging and clinical populations (Ali et al., 2011; Cadenas and Davies, 2000; González-Casacuberta et al., 2019; Hara et al., 2014; Kann and Kovács, 2007; Sun et al., 2013; Vos et al., 2010; Wang et al., 2014). This is of particular interest in the context of chronic immuno-compromised states as seen in PLWH, as the mitochondrial redox environment is also essential for carrying out normative immune responses to invading pathogens (Akkaya et al., 2018; Franchina et al., 2018; Sena et al., 2013; van der Windt et al., 2012) and is aberrant despite virologic suppression in PLWH (Spooner et al., 2021d). Importantly, prior work from our group has linked parameters of the mitochondrial redox environment to the cortical oscillations serving motor control in a sample of healthy adults (Spooner et al., 2021b). Essentially, we observed that parameters sensitive to superoxide in the periphery (i.e., intracellular superoxide levels, mitochondrial energetic capacity, superoxide dismutase activity), but not hydrogen peroxide (H_2O_2; i.e., catalase activity, glutathione reducing capacity), were robust predictors of planning- and execution-related beta oscillations in the contralateral M1. Further, increasing levels of superoxide and its scavenger, SOD, were robust mediators of the relationship between mitochondrial energetics and sensorimotor brain-behavior relationships (i.e., how well brain function predicts performance). While this study provided novel mechanistic insight regarding the modulation of optimal oscillatory profiles that govern *better* motor performance in healthy systems, the role of the mitochondrial redox environment in altering motor control in those exhibiting motor dysfunction (i.e., PLWH) is less well understood.

Thus, the goal of the current study was to evaluate the predictive capacity of mitochondrial-redox parameters, known to be disrupted in PLWH (Spooner et al., 2021d), on the peri-movement neural oscillations serving motor control in a cohort of virally-suppressed PLWH and demographically-matched uninfected controls. To this end, we employed advanced systems biology and neuroscience approaches including using the Seahorse Analyzer to assess mitochondrial respiration, electron paramagnetic resonance (EPR) spectroscopy of whole blood to quantify intracellular superoxide levels, antioxidant activity assays, and MEG imaging to directly quantify neural oscillatory activity during a motor sequence task. Based on prior studies (Spooner et al., 2021b, Spooner et al., 2021d), we used group-based path analysis and direct comparisons of unstandardized coefficients for each predictive path to test the following hypotheses: first, mitochondrial energetic capacities (i.e., adaptability to changing energetic demands) would differentially predict parameters of the redox environment sensitive to superoxide (i.e., superoxide levels, SOD activity) and H_2O_2-mechanisms (i.e., catalase activity, glutathione reducing capacities), and second, that features sensitive to superoxide mechanisms in the system, but not H_2O_2, would differentially predict the neural oscillatory dynamics serving motor control (i.e., *peri*-movement beta oscillations, reaction time, movement duration) evaluated using MEG in PLWH compared to uninfected controls.

2. Materials and methods

2.1. Participant Demographics

Eighty adults (range: 20–66 years old; 40 PLWH and 40 controls) were enrolled. All PLWH were receiving effective cART and had viral suppression defined as <50 copies/mL. Exclusion criteria included any medical illness affecting CNS function (other than HIV), any psychiatric or neurological disorder diagnosed by a neurologist, clinical psychologist or psychiatrist (e.g., stroke, Alzheimer's disease, Parkinson's disease, epilepsy, schizophrenia, generalized anxiety disorder, current major depressive disorder, PTSD, autism, etc.), reliance on external medical devices (e.g., pacemaker), history of head trauma resulting in loss of consciousness for >5 min, current pregnancy, current substance use/dependence (i.e., less than monthly use of substances except for alcohol and tobacco based on an extensive substance use questionnaire and the NIDA Quick Screen), the use of most psychiatric and neurological medications (e.g., anticonvulsants, antipsychotics), and the MEG Center's standard criteria for ferromagnetic materials (e.g., participants must be free of excessive dental work and unremovable metal implants/jewelry). The two groups were also balanced on common psychotropic medication use such as SSRIs for mild anxiety and depression. Uninfected controls were enrolled to demographically match PLWH based on their age ($t(78) = 0.18$, $p = .86$), sex ($X^2 = 3.65$, $p = .10$), handedness ($X^2 = 0.16$, $p = .99$) and body mass index (BMI: $t(78) = -1.12$, $p = .27$; for a comprehensive list, see Table 1).

Table 1
Participant Demographics and Clinical Assessments. Relevant test statistics (i.e., standardized mean difference, chi-squared differences) and p-values are reported for continuous and categorical variables, respectively.

	Controls	*PLWH*	*Test Statistic*	*p-value*
Demographics (Mean ± SD)				
N	40	40	–	–
Age (yrs)	45.1 ± 13.9	44.5 ± 13.8	0.03	0.86
Sex (% males)	57.5	77.5	3.65	0.10
Handedness (% right handed)	92.5	90.0	0.16	0.99
BMI (kg/m^2)	27.9 ± 5.6	29.3 ± 6.0	−0.18	0.27
CD4 Nadir (cells/μL)	–	282 ± 232	–	–
Current CD4 (cells/μL)	–	768 ± 322	–	–
Time since diagnosis (yrs)	–	12.8 ± 9.1	–	–
Time on ART (yrs)	–	10.1 ± 7.1	–	–

2.2. Experimental paradigm

Participants were seated in a nonmagnetic chair with their head positioned within the MEG helmet-shaped sensor array. Participants were initially asked to fixate on a crosshair for 3750 ms (±350 ms), followed by a presentation of three numbers for 500 ms, each corresponding to a finger on the hand (Fig. 1). Upon the presentation of a visual cue (i.e., numbers turning blue), participants were asked to tap the fingers corresponding to the numbers sequentially and given 2250 ms to complete the movement. A total of 160 trials were completed, making the overall recording time approximately 17 min.

For each participant, reaction time (RT: the time to respond to the first number in the sequence) and movement duration (MD: the time to complete the entire motor sequence) data were extracted for each trial and incorrect trials were excluded from all analyses. In addition, individual trial data was initially rejected based on behavioral performance metrics that exceeded a standard threshold that would ultimately impact MEG data analyses (i.e., RT > 1250 ms and MD > 3000 ms). The remaining RT and MD data was then averaged per participant and subjected to subsequent statistical analyses including structural equation modeling.

2.3. MEG data acquisition and coregistration with structural MRI

All recordings were performed in a one-layer magnetically-shielded room with active shielding engaged for environmental noise compensation. With an acquisition bandwidth of 0.1–330 Hz, neuromagnetic responses were sampled continuously at 1 kHz using a MEGIN/Elekta MEG system (MEGIN, Helsinki, Finland) with 306 magnetic sensors, including 204 planar gradiometers and 102 magnetometers. Throughout data acquisition, participants were monitored using a real-time audio–video feed from inside the magnetically-shielded room. MEG data from each participant were individually corrected for head motion and subjected to noise reduction using the signal space separation method with a temporal extension (Taulu and Simola, 2006). Each participant's MEG data were coregistered with their structural T1-weighted MRI data prior to imaging analyses using BESA MRI (Version 2.0). Structural MRI data were aligned parallel to the anterior and posterior commissures and transformed into standardized space. After beamformer analysis (see below), each subject's functional images were transformed into standardized space using the transform that was previously applied to the structural MRI volume and spatially resampled.

2.4. MEG preprocessing and sensor-level statistics

Cardiac and ocular artifacts were removed from the data using signal-space projection (SSP) and the projection operator was accounted for during source reconstruction (Uusitalo and Ilmoniemi, 1997). Epochs of 6150 ms duration were defined (i.e., −2050 to 4100 ms) with 0 ms defined as movement onset and the baseline being the −2050 to −1550 ms window. We rejected trials based on having a reaction time longer than 1250 ms or taking >3000 ms to complete the entire motor sequence, which would disrupt the baseline period. Next, remaining epochs containing artifacts were rejected based on a fixed threshold method, supplemented with visual inspection. On average, 127 trials per participant were used for further analysis and the number of accepted trials did not differ by group.

Artifact-free epochs were transformed into the time–frequency domain using complex demodulation (Kovach and Gander, 2016), and the resulting spectral power estimations per sensor were averaged over trials to generate time–frequency plots of mean spectral density. The sensor-level data per time–frequency bin were normalized using the

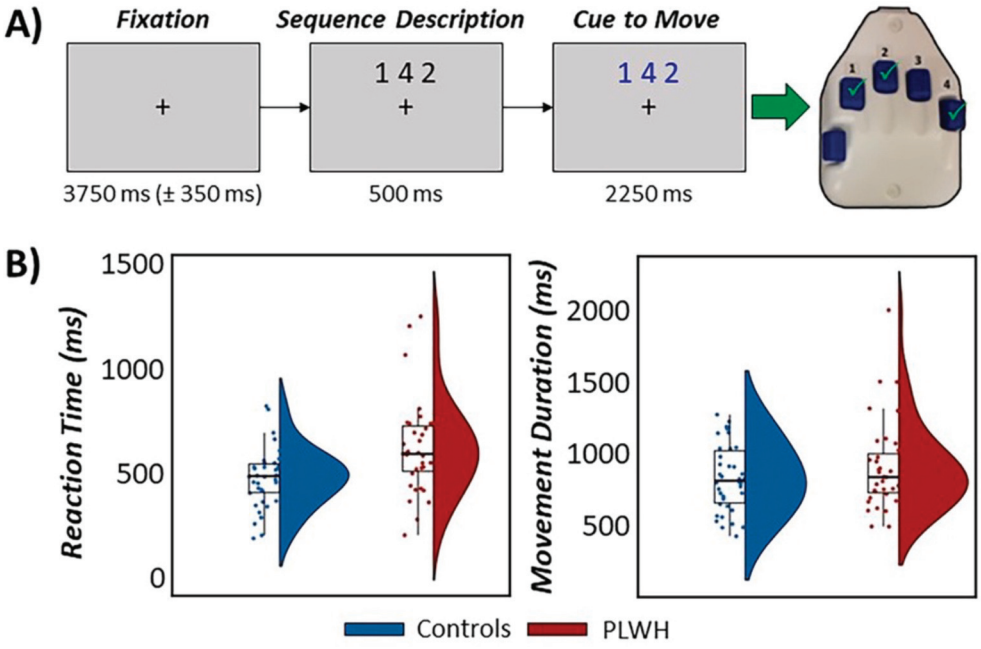

Fig. 1. Motor Sequence Paradigm and Behavioral Performance. (A): Participants were instructed to fixate centrally on a crosshair for 3750 ms (±350 ms), followed by a sequence description in black (500 ms) consisting of three numbers that corresponded to fingers on the right hand. The cue to move was denoted by the numbers changing colors to blue. Participants were instructed to tap the sequence in order as quickly as possible with the right-handed button pad. (B): PLWH shown in red were slower to respond to the first number in the sequence (i.e., reaction time) compared to healthy controls (shown in blue). Movement duration (i.e., time to complete the entire motor sequence) did not differ between groups.

mean power per frequency during the −2050 to −1550 ms baseline period. The specific time–frequency windows used for imaging were determined through a two-stage, data-driven approach involving statistical analysis of the sensor-level spectrograms across all participants (i.e., PLWH *and* healthy controls) and trials. First, paired-sample t-tests against baseline were conducted on each data point, with the output spectrogram of *t*-values initially thresholded at $p < .05$ to define time–frequency bins containing potentially significant oscillatory deviations. To reduce the risk of false positive results due to multiple comparisons, the time–frequency bins that survived this initial threshold were temporally and/or spectrally clustered with neighboring bins that were also significant, and a cluster value was derived by summing all of the *t*-values of all data points in the cluster. Nonparametric permutation testing (10,000 permutations) was then used to derive a distribution of cluster values and the significance level of the observed clusters were tested directly using this distribution. Based on this analysis, the time–frequency periods that contained significant oscillatory events across all participants and were relevant to our primary hypotheses (i.e., *peri*-movement beta activity) were subjected to beamforming analyses. Of note, in the case of the temporally-sustained *peri*-movement beta oscillations, we focused on a window surrounding the peak of the response (i.e., greatest amplitude fluctuation from baseline) in order to optimize the signal-to-noise ratio and selected equally-sized 500 ms temporal windows for the motor planning and execution periods to facilitate interpretation of the findings. Note that the significant time–frequency extent of the *peri*-movement beta response was identified across *all participants* (i.e., PLWH *and* healthy controls) to ensure that potential group differences in brain-behavior relationships tested in our structural equation models would not be biased due to asymmetrical definitions of time–frequency windows, which would ultimately contribute to subsequent differences in signal-to-noise ratios per oscillatory response per group. Further details on this method and our processing pipeline can be found in recent papers (Heinrichs-Graham et al., 2020; Spooner et al., 2021a, 2021b, 2021c, 2021d; Spooner et al., 2020a, 2020b; Wiesman et al., 2020).

2.5. MEG source imaging

Cortical oscillatory networks were imaged through the dynamic imaging of coherent sources (DICS) beamformer (Gross et al., 2001), which uses the cross-spectral density matrices to calculate source power for the entire brain volume. These images are typically referred to as pseudo-t maps, with units (pseudo-t) that reflect noise-normalized power differences (i.e., active vs passive) per voxel. Following convention, we computed noise-normalized, source power per voxel in each participant using baseline periods of equal duration and bandwidth (Hillebrand et al., 2005). MEG preprocessing and imaging used the Brain Electrical Source Analysis (Version 7.0; BESA) software.

Normalized source power was computed over the entire brain volume per participant at $4.0 \times 4.0 \times 4.0$ mm resolution for the time–frequency periods identified through the sensor level analyses. Prior to statistical analysis, each participant's MEG data, which were coregistered to native space structural MRI prior to beamforming, were transformed into standardized space using the transform previously applied to the structural MRI volume and spatially resampled. The resulting 3D maps of brain activity were averaged across all participants to assess the neuroanatomical basis of the significant oscillatory responses identified through the sensor-level analysis. Source power was then extracted from peak voxels per time bin (i.e., planning and execution phases) per participant and underwent statistical modeling.

2.6. Isolation of peripheral blood mononuclear cells and respiration analysis

Whole blood was collected into EDTA tubes by venous puncture for all participants. Buffy coats were submitted to a Ficoll-Paque Plus (GE Healthcare) gradient centrifugation for isolation of the mononuclear fraction. PBMCs were cryopreserved in Fetal Bovine Serum with 10 % DMSO. Cells were thawed within 6 weeks of isolation and underwent assessment using the Seahorse XF96 Analyzer (Seahorse Bioscience) to quantify oxygen consumption rate (OCR) using the mitochondrial stress test assay. Specifically, PBMCs were plated at 500,000 cells/well and 3 OCR measurements were taken sequentially on 5–6 technical replicate wells prior to and upon serial injection of 3.5 μM oligomycin (Sigma; complex V inhibitor), 1 μM fluoro-carbonyl cyanide phenylhydrazone (FCCP; Sigma; mitochondrial oxidative phosphorylation uncoupler) and 14 μM rotenone + 14 μM antimycin A (Sigma; complex I and III inhibitors, respectively) to evaluate measures of mitochondrial respiration including basal respiration, ATP-linked respiration, proton leak, maximal respiration, spare respiratory capacity (SRC) and non-mitochondrial respiration. All bioenergetic data were normalized to protein in the well for subsequent analyses. For data calculation, the Seahorse Wave software (v2.2.0) was used.

2.7. Quantification of the redox environment

Cellular levels of superoxide were assessed using electron paramagnetic resonance (EPR) spectroscopy of whole blood incubated with a superoxide-sensitive spin probe (1-hydroxy-3-methoxycarbonyl1-2,2,5,5-tetramethylpyrrolidine: CMH) for 1 h under physiologic conditions (37C), as previously described (Ahmad et al., 2016; Spooner et al., 2021b, Spooner et al., 2021d). Specifically, immediately after sample collection, 200 μM of CMH was reconstituted into EPR buffer (Krebs Hepes Buffer) supplemented with metal chelators (5 μM sodium diethyldithiocarbamate trihydrate and 25 μM deferoxamine) and incubated with 200 μL of whole blood. EPR measurements were performed with a Bruker eScan EPR spectrometer (Bruker BioSpin GmbH, Rheinstetten/Karlsruhe, Germany), with the following parameters: field sweep width, 100.0 G; center field, 3482 G; microwave frequency, 9.75 kHz; microwave power, 1.10 mW; modulation amplitude, 5.94 G; conversion time, 10.24 ms; time constant, 40.96 ms. The resulting EPR spectra amplitude is expressed as arbitrary units (a.u.) that are directly proportional to the amount of total cellular superoxide in the sample. Of note, due to the cell permeability of CMH allowing for the detection of superoxide within subcellular compartments (e.g., mitochondria), we may presume that the levels of superoxide reacting with CMH in the current study originated from these subcellular compartments such as the mitochondria (Ahmad et al., 2016; Spooner et al., 2021b, Spooner et al., 2021d). It should also be noted that CMH may react with extracellular superoxide prior to permeating cell membranes.

Antioxidant activity levels were quantified in erythrocytes for key enzymatic and non-enzymatic contributors to the mitochondrial redox environment, including superoxide dismutase (SOD), catalase, and glutathione. Specifically, we used the SOD Assay Kit-WST (DOJINDO, Inc.) to measure total SOD activity, the OxiSelect Catalase Activity Assay Kit (Cell Biolabs, Inc.) for catalase, and the GSSG/GSH Quantification kit (DOJINDO, Inc.) for total (tGSH), oxidized (GSSG), and reduced glutathione (GSH) according to the manufacturers' guidelines.

2.8. Statistical analysis

All statistical analyses were performed following standard data trimming procedures whereby measures that exceeded 2.5 standard deviations above or below the group's mean were excluded from subsequent analyses. First, we aimed to evaluate changes in behavioral performance metrics (i.e., accuracy, reaction time, movement duration) as a function of group using independent-samples t-tests between PLWH and uninfected controls. Next, to evaluate the predictive capacity of the mitochondrial redox environment on movement-related neural oscillations serving behavior, we conducted a group-based path analysis, which provides parameter estimates simultaneously for PLWH versus uninfected controls (all two-tailed *p*-values reported). Our primary

hypotheses were that movement-related beta oscillatory activity during planning and execution phases of movement would predict task performance, and that these dynamics would be differentially modulated by the mitochondrial redox environment as a function of serostatus. Predictive capacities of each path were evaluated by direct comparisons of unstandardized coefficients in PLWH versus controls. In addition, we conducted a multiple mediation model whereby measures of mitochondrial function (i.e., spare respiratory capacity) predicted movement-related oscillations and subsequent behavioral performance through changes in the redox environment (i.e., superoxide, SOD, catalase, GSSG/tGSH ratio) for superoxide-sensitive and H_2O_2-sensitive paths, separately. Importantly, we examined the 95 % confidence intervals of bias-corrected bootstrapped confidence intervals based on 1000 bootstrapped samples (Efron and Tibshirani, 1986), which provides a robust estimate of asymmetrical mediation effects (Fritz and MacKinnon, 2007). All analyses were conducted with full information maximum likelihood estimation for missing data using MPlus (v.8.1).

3. Study approval

The University of Nebraska Medical Center Institutional Review Board approved the study and all participants provided written informed consent.

4. Results

4.1. Sequential movement performance

Following initial rejection of trials exceeding behavioral performance metrics that would impact MEG data analyses (i.e., reaction times > 1250 ms; movement durations > 3000 ms), an average of 127 trials per participant remained for subsequent statistical modeling. Participants performed generally well on the task, with an average accuracy of 92.71 % (Controls: 93.92 ± 4.76 %; PLWH: 91.41 ± 10.81 %), which did not differ as a function of group (p =.195). In contrast, reaction time (i.e., response time to the first button press) was significantly slower for PLWH (620.89 ± 224.24 ms) compared to uninfected controls (479.17 ± 139.76 ms; p =.002; Fig. 1). Finally, movement duration (i.e., time to complete the entire motor sequence) did not significantly differ as a function of HIV infection (Controls: 831.44 ± 234.47 ms; PLWH: 907.74 ± 312.70 ms; p =.240; Fig. 1).

4.2. MEG sensor- and source-level analyses

Time-frequency analyses locked to the first movement in the sequence indicated significant *peri*- and post-movement oscillatory responses in gradiometers near the contralateral sensorimotor strip across all participants regardless of group (p <.001, Fig. 2). Specifically, decreases in *peri*-movement beta activity (16–26 Hz) were observed prior to and following movement (i.e., −500 to 0 ms and 0 to 500 ms for planning and execution, respectively). In addition, we observed transient increases in theta oscillatory activity surrounding movement onset, while more sustained decreases during movement onset were observed in the alpha range (Fig. 2). Finally, we observed post-movement increases in beta activity following motor execution. However, given our hypotheses, *peri*-movement oscillations in the theta and alpha range, as well as post-movement oscillations in the beta range were outside the scope of this study and did not undergo source imaging analyses.

To identify the neural origins of oscillations seen at the sensor level, planning and execution phases were imaged separately using a beamformer. The resulting maps indicated that pre-movement decreases in beta power were the strongest in left M1 contralateral to movement (i.e., −500–0 ms, Fig. 2), while more bilateral decreases in beta power were observed during the execution phase of movement (i.e., 0–500 ms), regardless of group. Peak voxel values (i.e., pseudo-t) were then extracted from the left M1 per time bin and underwent subsequent statistical modeling.

4.3. Superoxide-sensitive redox environments mediate brain-behavior dynamics in controls, but not in PLWH

As described in the methods, we tested a multiple mediation model using a group-based path analysis to determine the direct effect of superoxide-sensitive features of the mitochondrial redox environment (i.e., SRC, superoxide, SOD) on brain-behavior relationships serving motor performance, which simultaneously calculated the effects for PLWH versus uninfected controls. In addition, direct comparisons of unstandardized coefficients were assessed per predictive path to identify

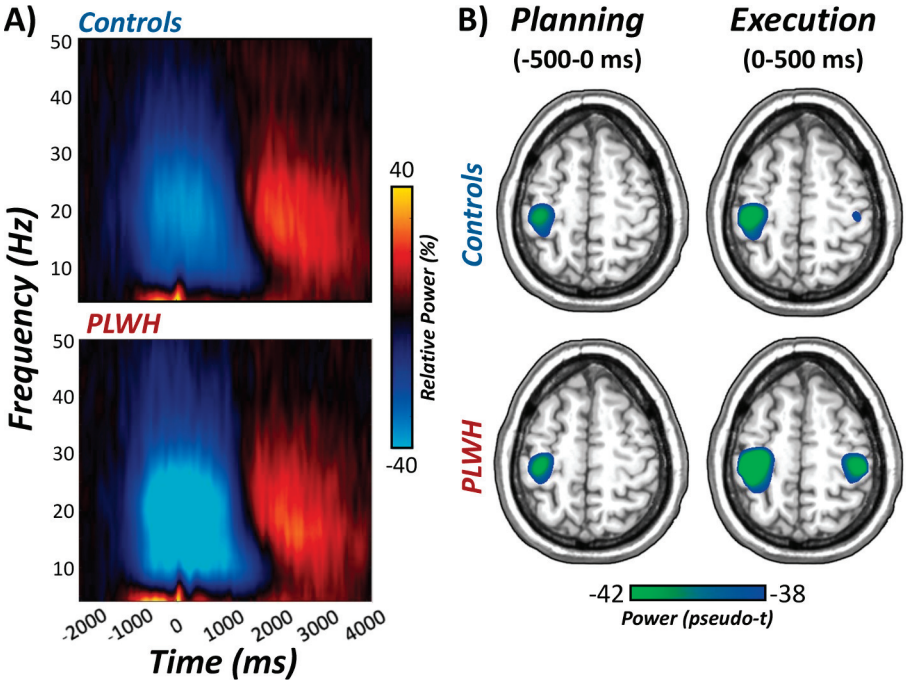

Fig. 2. Sensor- and Anatomical-Space Movement-related Oscillations. (A): Time frequency spectrograms locked to the onset of the first movement in the sequence (0 ms) for a sensor near the left sensorimotor cortex averaged for controls (top) and PLWH (bottom). The x-axis denotes time (in ms) and the y-axis denotes frequency (in Hz). Relative power (i.e., percent change from baseline −2050 to −1550 ms) is expressed according to the color scale bar to the right of the graphic. (B): Significant movement-related oscillations were imaged using a beamformer for planning and execution phases, separately. Strong decreases in beta activity (16–26 Hz) were observed in the contralateral M1 during motor planning (−500–0 ms), with identical peak voxel locations for PLWH and controls. In addition, strong beta decreases were observed bilaterally for PLWH and controls during motor execution (0–500 ms).

differences as a function of group. Our brain-behavior relationships included paths whereby beta oscillatory activity during the planning period (-500 to 0 ms) predicted reaction time, as well as beta activity during motor execution (0 to 500 ms). Variables during planning and execution phases then predicted movement duration (i.e., time to complete the entire sequence). Finally, we simultaneously modeled shared covariance between features of the redox environment (i.e., superoxide concentration and SOD activity), as well as brain-behavioral features occurring synchronously in time (i.e., reaction time and beta oscillations during motor execution). For a full model visualization, see Fig. 3.

To begin, we found a robust relationship between reaction time and movement duration on the task, such that faster responses to the first number in the sequence led to faster sequence completion time for PLWH ($\beta = 0.59$, $p < .001$) and uninfected controls ($\beta = 0.51$, $p = .001$). In addition, as expected, beta activity during the planning period was related to activity during the execution phase in the left M1 (contralateral to movement) in both groups (Controls: $\beta = 1.0$, $p < .001$; PLWH: $\beta = 0.96$, $p < .001$). Interestingly, *peri*-movement beta activity did not significantly relate to reaction time nor movement duration in either group ($ps > 0.109$).

In regard to superoxide-sensitive redox environments, uninfected controls exhibited a robust relationship between mitochondrial SRC, superoxide and its scavenger (SOD), such that decreases in SRC were associated with increased levels of cellular superoxide ($\beta = -0.41$, $p = .005$), and reduced levels of total SOD activity ($\beta = 0.38$, $p = .013$). Contrary to these relationships in controls, PLWH only exhibited marginal associations among mitochondrial SRC and superoxide, such that increased mitochondrial energetic reserve was marginally associated with increased levels of superoxide ($\beta = 0.27$, $p = .087$). Importantly, these data suggest an immediate separable pattern of the influence of mitochondrial energetics on superoxide-sensitive redox parameters between PLWH and uninfected controls.

In regard to the influence of the mitochondrial redox environment on brain-behavior dynamics, we observed no direct effects of mitochondrial function on *peri*-movement oscillatory activity in the contralateral M1 ($ps > 0.105$), although decreases in SRC were associated with faster reaction times in controls ($\beta = 0.39$, $p = .035$; Fig. 3). In contrast, we observed robust direct effects of the redox environment on brain and behavior relationships (Fig. 3). Briefly, among uninfected controls, levels of cellular superoxide significantly modulated beta activity during motor execution ($\beta = -0.12$, $p = .007$), while increased activity levels of superoxide's scavenger (i.e., SOD) were associated with weaker planning-related decreases in the left M1 ($\beta = 0.43$, $p = .008$) and faster reaction times ($\beta = -0.48$, $p = .006$) on the motor sequence task. In contrast, only cellular levels of superoxide significantly modulated execution-related beta oscillations in PLWH, such that increased levels of superoxide were associated with stronger beta decreases during motor execution ($\beta = -0.15$, $p = .002$).

Next, we examined all potential mediating effects of the redox environment on mitochondrial-related changes in motor cortical dynamics and behavioral performance. As described in the methods, statistical significance of indirect effects was determined by using bias-corrected bootstrapped confidence intervals using 1000 bootstrapped samples (Efron and Tibshirani, 1986; Fritz and MacKinnon, 2007), thus exact *p*-values are not available for indirect effects. We observed five statistically significant indirect effects ($p < .05$) for uninfected controls, which implicated levels of superoxide as strong mediators of bioenergetic-neural pathways involved in motor execution, while SOD activity mediated this change during the planning phase of movement (see Table 2). Further, we observed that superoxide-sensitive features of the redox environment and mitochondrial function together accounted for 34.9 % of the variance in the brain-behavior dynamics serving sensorimotor performance in healthy controls ($p < .001$).

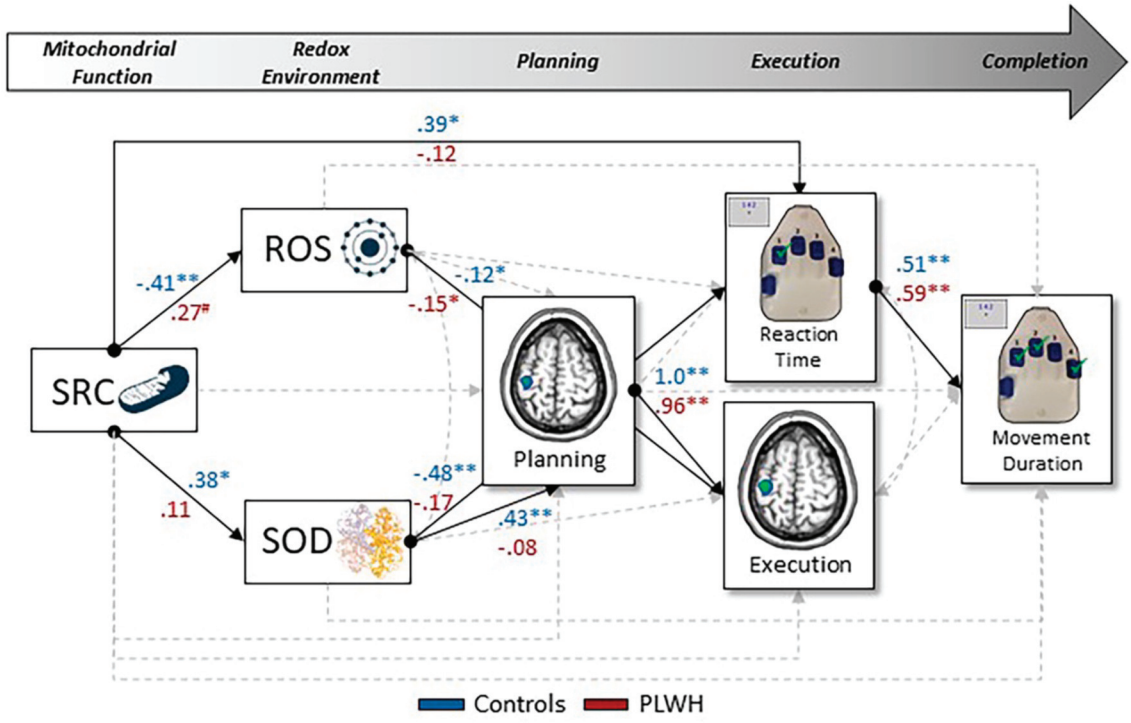

Fig. 3. Superoxide-Sensitive Parameters Differentially Modulate Sensorimotor Performance in PLWH. Results of the group-based path analysis of the predictive capacity of superoxide-sensitive features of the mitochondrial redox environment on movement-related oscillations and behavior in PLWH versus uninfected controls. Single-headed arrows denote predictive paths and double-headed arrows denote correlations. Statistically significant estimates ($p < .05$) are denoted with solid lines, while non-significant paths are denoted with dashed gray lines. All listed parameters are standardized coefficients for controls in blue and PLWH in red. Together, superoxide-sensitive pathways accounted for 34.9 % and 52.8 % of the variance in movement duration for controls and PLWH, respectively. $^{\#}p < .10$, $^{*}p < .05$, $^{**}p < .005$.

Table 2
Results of the Group-based Mediation Analyses using Structural Equation Modeling. Indirect effects were assessed for statistical significance using the bias-corrected bootstrapped confidence intervals. Significant indirect effects are bolded for visualization. All reported parameters are standardized coefficients. *p <.05. SRC: spare respiratory capacity; SOD: superoxide dismutase; RT: reaction time; MD: movement duration; EPR: superoxide concentration; Plan: planning-related beta activity; Exec: execution-related beta activity.

Controls				***PLWH***			
Mitochondrial SRC to Movement Duration							
Path	**Total**	**Direct**	**Indirect**	**Path**	**Total**	**Direct**	**Indirect**
SRC → SOD → RT → MD	0.13	0.02	**−0.09***	SRC → SOD → RT → MD	−0.41*	−0.25	−0.01
Mitochondrial SRC to Reaction Time							
SRC → SOD → RT	0.16*	0.39*	**−0.18***	SRC → SOD → RT	−0.23	−0.11	−0.01
Mitochondrial SRC to Motor Execution							
SRC → EPR → Exec	−0.13*	−0.08*	**0.05***	SRC → EPR → Exec	0.09	0.01	−0.04
SRC → SOD → Plan → Exec	−0.13*	−0.08*	**0.16***	SRC → SOD → Plan → Exec	0.09	0.01	−0.09
Mitochondrial SRC to Motor Planning							
SRC → SOD → Plan	−0.09	−0.19*	**0.16***	SRC → SOD → Plan	0.13	0.14	−0.01

In contrast, we observed no mediating effects of the redox environment on these bioenergetic-neural pathways in PLWH, suggesting an uncoupling of the redox environment to differentially modulate sensorimotor brain-behavior dynamics in PLWH (see Table 2). Nevertheless, we evaluated whether the predictive capacities of these relationships differed as a function of group by directly comparing the unstandardized coefficients associated with each path. Interestingly, this analysis confirmed different predictive capacities of the relationships between mitochondrial SRC and superoxide ($\Delta b = 0.03$, $p = .005$), as well as SOD activity and planning-related beta responses in the left M1 ($\Delta b = -9.38$, $p = .031$) in PLWH versus uninfected controls. Importantly, these parameters sensitive to superoxide redox mechanisms in the system explained 52.8 % of the variance in movement duration in virally-suppressed PLWH ($p < .001$).

4.4. H_2O_2-sensitive pathways relate to sensorimotor Brain-Behavior dynamics in PLWH, but not controls

Next, we evaluated the predictive capacity of H_2O_2-sensitive redox environments and mitochondrial function on brain-behavior relationships serving sensorimotor control using group-based path analyses. Importantly, our measures of the redox environment were now comprised of catalase activity and GSSG/tGSH ratios as continuous predictors of movement-related beta activity during motor planning and execution phases, as well as behavior on the task. Finally, we simultaneously modeled shared covariance between features of the redox environment (i.e., catalase activity and GSSG/tGSH ratios), as well as brain-behavioral features occurring synchronously in time (i.e., reaction time and beta oscillations during motor execution). For full model visualization, see Fig. 4.

Similar to our superoxide-sensitive model, reaction time was strongly related to movement duration in both groups (Controls: $\beta = 0.49$, $p = .001$; PLWH: $\beta = 0.60$, $p < .001$; Fig. 4). Likewise, planning-

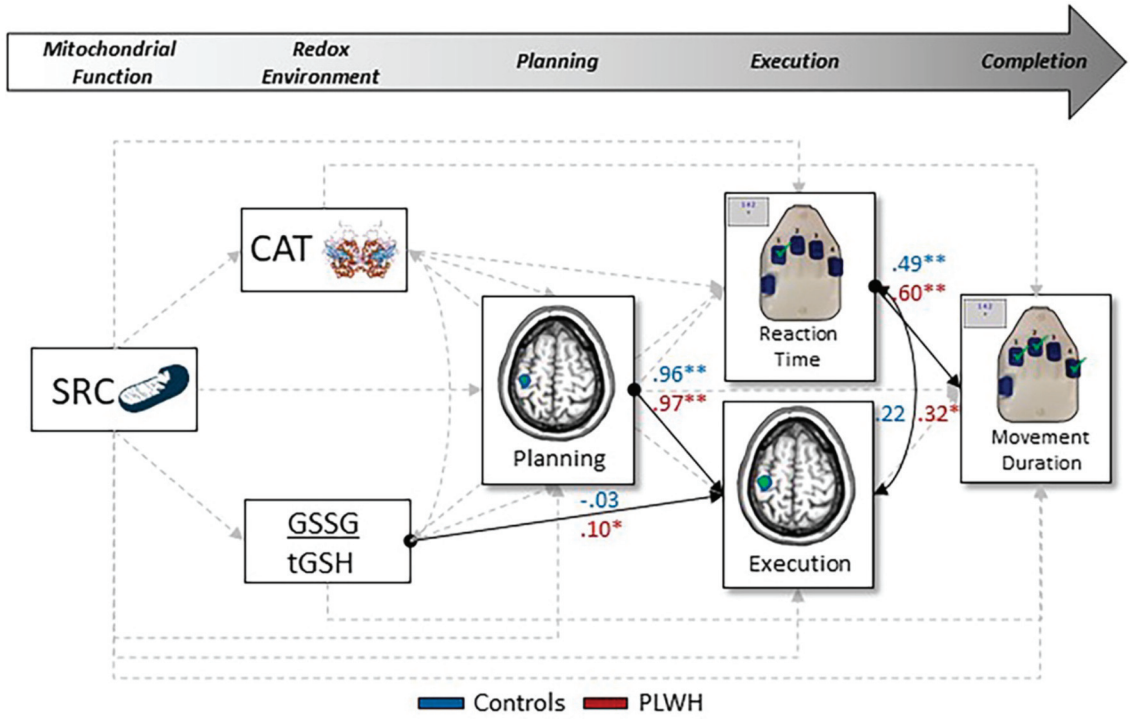

Fig. 4. H_2O_2-Pertinent Antioxidants Differentially Predict Sensorimotor Brain-Behavior in PLWH. Single-headed arrows denote predictive paths and double-headed arrows denote correlations. Statistically significant estimates (p <.05) are denoted with solid lines, while non-significant paths are denoted with dashed gray lines. All listed parameters are standardized coefficients for PLWH in red and healthy controls in blue. *p <.05, **p <.005.

related decreases in M1 beta power led to strong execution-related beta decreases regardless of group (Controls: $\beta = 0.96$, $p < .001$; PLWH: $\beta = 0.97$, $p < .001$). Interestingly, we observed no direct effects of mitochondrial SRC nor H_2O_2-sensitive antioxidants on brain-behavior relationships serving motor function in healthy controls (Fig. 4). In addition, we observed no mediating effects of the redox environment between mitochondrial function and brain-behavior relationships.

In contrast, PLWH exhibited a direct effect of mitochondrial energetic capacity on movement duration ($\beta = -0.30$, $p = .027$), such that decreased SRC was associated with longer time to complete the entire motor sequence. In addition, PLWH demonstrated a significant association among GSSG/tGSH ratios and execution-related beta decreases in the left M1 ($\beta = 0.10$, $p = .040$), such that attenuated glutathione reducing capacities (i.e., higher GSSG/tGSH ratio) were associated with stronger beta decreases during motor execution in the contralateral left M1 (Fig. 4). Interestingly, we observed no significant mediating effects of H_2O_2-pertinent redox parameters in PLWH. However, direct comparisons between the unstandardized coefficients of each direct path revealed significantly different predictive capacities between PLWH and uninfected controls in the relationships among mitochondrial SRC and movement duration ($\Delta b = -55.66$, $p = .035$) and glutathione reducing capacity (i.e., GSSG/tGSH ratios) and movement execution ($\Delta b = 7.92$, $p = .041$), suggesting a differential coupling of these H_2O_2-pertinent redox parameters with brain and behavior in PLWH versus their uninfected counterparts.

5. Discussion

In the current study, we used advanced neurophysiology and systems biology approaches to determine the predictive capacity of the mitochondrial redox environment on sensorimotor brain-behavior dynamics in a cohort of virally-suppressed PLWH and demographically matched uninfected controls. Specifically, we observed differential effects of superoxide-sensitive redox parameters, such that in uninfected controls, increases in superoxide and SOD activity levels were robust modulators of execution-related and planning-related beta oscillations in the contralateral M1, respectively, while only intracellular levels of superoxide were strongly associated with execution-related beta power in PLWH. In addition, superoxide and SOD were strong mediators of the relationship between mitochondrial SRC and brain-behavior relationships serving motor control in seronegative participants, while we observed no mediating effects of the redox environment in PLWH, suggesting a bioenergetic-neural uncoupling as a function of serostatus. Finally, our data suggest H_2O_2-sensitive mechanisms are direct modulators of sensorimotor neural dynamics in PLWH, but not in uninfected controls. Below, we discuss the implications of these novel findings for understanding the contribution of the mitochondrial redox environment in HIV infection and sensorimotor control.

Our most important finding was likely the contribution of superoxide-sensitive parameters of the redox environment on brain-behavior relationships serving sensorimotor control in PLWH. Briefly, increases in SOD and superoxide were associated with weaker planning- and execution-related beta oscillations in M1 of uninfected controls, respectively. In contrast, only intracellular levels of superoxide were significant modulators of execution-related neural oscillations in PLWH, such that elevated levels of superoxide were associated with stronger movement-related beta oscillations. In addition, decreases in mitochondrial SRC were related to slower sequence completion times on the task in seropositive adults. This is an important distinction between normative and pathological systems, as in uninfected controls, these results coincided with a well-established pattern of brain-behavior dynamics that typically govern healthy motor function.

Essentially, weaker M1 beta oscillations during the planning period led to weaker beta power during motor execution and better task performance (i.e., faster movement durations (Heinrichs-Graham et al., 2018a; Heinrichs-Graham et al., 2018b; Heinrichs-Graham and Wilson, 2016)). Of note, it was not surprising that M1 beta oscillations were not associated with changes in reaction times for either group based on previous studies using this task paradigm (Heinrichs-Graham and Wilson, 2016, 2015; Spooner et al., 2021b). Essentially, due to the nature of the task design, which carefully controlled for numerous factors likely reflecting changes in both motor and cognitive components of the motor plan (e.g., number of movements performed, possible movement options, muscle groups engaged; i.e., reaction time (Hohle, 1965)), it is possible that our motor sequence paradigm was less sensitive to characterizing changes in reaction time as opposed to the execution- and completion-related behavioral components tested (i.e., movement duration). Nevertheless, we observed that the relationship among beta power in the contralateral M1 and behavior was absent in PLWH and further, our data suggest that disparate increases in superoxide and decreases in mitochondrial energetic capacity (i.e., SRC) led to less optimal oscillatory-behavioral profiles (i.e., stronger beta decreases, worse performance on the task, respectively). However, it is important to note that our lack of relationship between M1 beta oscillatory dynamics and behavior in PLWH could be attributable at least in part to the fact that we interrogated the oscillatory dynamics within M1, as opposed to other regions that comprise the extended sensorimotor network. In fact, numerous studies suggest that the parietal cortices are superior predictors of sequence-related motor performance above and beyond M1-involvement alone (Heinrichs-Graham et al., 2020; Heinrichs-Graham and Wilson, 2015; Samuel et al., 1997; Yokoi and Diedrichsen, 2019). This is also corroborated by the notion that PLWH typically exhibit a greater degree of activation relative to uninfected controls in association cortices (i.e., prefrontal and parietal cortices) during task performance, often reflecting a mechanism employed by seropositive adults to compensate for less efficient neural systems to achieve task demands (Chang et al., 2008, 2004; Ernst et al., 2009, Ernst et al., 2002). Thus, the study of beta oscillations within the parietal cortices may provide unique insight into aberrant motor sequence performance and importantly, its differential modulation by the mitochondrial redox environment in seropositive adults.

The notion that superoxide-sensitive redox parameters are pertinent to sensorimotor function is not new, although this line of research has only been successfully interrogated in animal models. Essentially, using SOD knockout models (i.e., cytosolic isoforms of SOD; SOD1), investigators have genetically mutated SOD1 in the system, which leads to dramatic depletions in SOD activity levels and subsequent increases in superoxide, giving rise to a host of motor deficits observed most commonly in animal models of neurodegeneration (e.g., ALS; Johnson and Giulivi, 2005; Reaume et al., 1996; Sims-Robinson et al., 2013). In addition, SOD depletion may also cause death depending on the targeted isoform (i.e., mitochondrial isoforms of SOD, SOD2; Fukui and Zhu, 2010)). Thus, it is clear that alterations in SOD activity may play an important, and *early* role in neural and behavioral processing. This notion is corroborated by our findings of differential impacts of SOD and superoxide concentrations on planning- and execution-related changes under normal physiologic conditions (i.e., healthy controls), respectively; which could suggest an early influence of SOD that may impact downstream processing when presented with less-optimal or aberrant physiologic conditions (e.g., HIV exposure). Importantly, while our data suggest that healthy systems (i.e., uninfected controls) exhibit mechanistic increases in superoxide and SOD to govern more *optimal* brain-behavior profiles in humans, deficient mitochondrial respiration and, alternatively, increases in superoxide were associated with worse brain-behavior dynamics serving sensorimotor function in PLWH, perhaps reflective of similar neurodegenerative properties present in seropositive adults. This relationship between mitochondrial bioenergetics and sensorimotor brain-behavior dynamics was also robustly mediated by levels of superoxide and SOD in healthy controls, while no mediating effects were observed in PLWH. The lack of bioenergetic-neural coupling in PLWH may be attributable, at least in part, to the disparate predictive capacities of the redox environment observed between our groups.

Essentially, we observed that deficiencies in the bioenergetic capacity of the mitochondria (i.e., reduced SRC) were related to decreased levels of superoxide in PLWH, which contradicts prior work in cART-treated and treatment-naïve humans and animal models (Avdoshina et al., 2016; Korencak et al., 2019; Shah and Kumar, 2016), albeit this result was not surprising and could be related to the cellular composition of our PBMC samples (Korencak et al., 2019; Spooner et al., 2021b, Spooner et al., 2021d). Nonetheless, this pattern of results points to dissociable, rather than dependent, mechanisms by which superoxide and mitochondrial respiration modulate brain and behavior in PLWH, as opposed to the robust coupling of the mitochondrial redox environment and optimal brain-behavior profiles in the seronegative population.

Finally, we observed a direct modulation of sensorimotor oscillatory dynamics by H_2O_2-pertinent antioxidants in the system in PLWH, which was not present in seronegative controls (Spooner et al., 2021b, Spooner et al., 2021d). Briefly, in virally-suppressed PLWH, attenuated glutathione reducing capacities (i.e., higher GSSG/tGSH ratios) were associated with stronger beta oscillations in the contralateral M1 during motor execution and importantly, direct comparisons of unstandardized coefficients revealed disparate predictive capacities of this relationship between PLWH and uninfected controls. This result was not surprising, as a depletion in peripheral glutathione levels has long been revered as a key marker of oxidative stress in HIV-infection (Gil et al., 2003; Pace and Leaf, 1995; Repetto et al., 1996), which was related to sub-optimal oscillatory recruitment (i.e., stronger beta oscillations) in the present study. Importantly, this study expands upon prior work, as the distinction between oxidizing, reducing and total forms of glutathione (i.e., GSSG, GSH, tGSH, respectively) had yet to be examined. This is unfortunate, as the study of disparate oxidative properties of glutathione provides unique insight into the reducing capacity of peroxides in the system above and beyond absolute levels of this cofactor alone. Nevertheless, it is important to note that future work will undoubtably benefit from the direct quantification of H_2O_2, along with the H_2O_2-sensitive scavengers as measured in the current study to better understand the link between H_2O_2 redox mechanisms and sensorimotor function in PLWH.

In conclusion, our study is the first to directly quantify features of mitochondrial function and the redox environment and directly link to the oscillatory neural dynamics serving motor control in virally-suppressed PLWH and uninfected controls. Importantly, our results provide evidence for a differential modulation of both superoxide- and H_2O_2-sensitive redox pathways on M1 beta oscillatory activity and motor sequence performance in PLWH, while only superoxide-sensitive features modulated brain-behavior dynamics in uninfected controls. However, future studies directly quantifying levels of H_2O_2 in the system will be of utmost importance, as the current study now sheds light on the involvement of H_2O_2-pertinent redox parameters in pathological sensorimotor dysfunction. Moreover, it is important to note that while the current study aimed to identify features sensitive to superoxide and H_2O_2 environments separately (i.e., superoxide/SOD and catalase/glutathione levels, respectively), there are certainly redox parameters pertinent to modulating *both* environments (e.g., SOD effectively reducing more reactive superoxide species to more stable H_2O_2 ones; Buettner, 2011)). Thus, it will be important for future work to fully elucidate the role of SOD in *both* environments, concomitant with the direct quantification of H_2O_2 to facilitate comparison with the approach employed herein for superoxide-sensitive environments. In addition, we observed disparate trajectories by which mitochondrial respiration related to changes in the redox environment in PLWH versus uninfected controls, including separable mechanisms of action among the mitochondria and superoxide-sensitive redox parameters in PLWH, as opposed to the dependency of the redox environment in mediating mitochondrial bioenergetic-neural relationships in controls (Spooner et al., 2021b). Although we can presume that the cellular levels of superoxide as measured in the current study may originate from the mitochondria due to the cell permeability of the superoxide-sensitive spin probe used for detection (i.e., CMH), future work will benefit from the direct quantification of these redox parameters within the mitochondria (e.g., mitochondrial isoform of SOD: MnSOD and superoxide levels from isolated mitochondria), to support the notion of mitochondrial-induced bioenergetic uncoupling in PLWH. Alternatively, evaluating other cellular sources of ROS (e.g., NOX enzymes; Lambeth, 2004)) and their relation to the superoxide redox environment as measured in the current study will be critical to fully unravel the source of redox-regulated neural oscillatory profiles in PLWH. Finally, while the current study was unique in that we studied a relatively large sample of *virally-suppressed* PLWH, previous studies have evaluated smaller samples of HIV-infected adults with and without virologic suppression. This is an important consideration, as patients with higher levels of viremia generally also have excessive inflammation and other ongoing pathological processes that may be associated with mitochondrial toxicity and subsequent redox imbalances independently. While the inclusion of virally-suppressed PLWH without psychiatric illnesses and other comorbidities is often considered a strength, as it minimizes the potential influence of confounding factors, it may limit the generalizability of our findings to PLWH presenting with numerous comorbidities (e.g., depression, psychiatric symptoms, substance use or dependence, etc.; Mimiaga et al., 2013; Rabkin, 2008)). Thus, future work may benefit from including patients with such comorbid conditions. Nonetheless, our data suggest that blood-based markers of mitochondrial function and the redox environment function as important modulators of beta oscillatory dynamics serving sensorimotor control in both healthy and pathological systems and further, may serve as targets for remedying motor dysfunction and cognitive decline in PLWH in the future.

Declaration of Competing Interest

The authors declare that they have no known competing financial interests or personal relationships that could have appeared to influence the work reported in this paper.

Data availability

Data will be made available on request.

Acknowledgments

This research was supported by grants R01-MH116782 (TWW), R01-MH118013 (TWW), R01-DA047828 (TWW), R01-DA056223 (TWW), P20-GM144641 (TWW), and T32-NS105594 (RKS) from the National Institutes of Health (NIH), and grant #1539067 from the National Science Foundation (TWW). EPR Spectroscopy data was collected in the University of Nebraska's EPR Spectroscopy Core, which was initially established with support from a Center of Biomedical Research Excellence grant from the National Institute of General Medical Sciences of the National Institutes of Health (P30-GM103335) awarded to the University of Nebraska's Redox Biology Center. We would like to thank all of the volunteers for participating in the study, as well as our staff and collaborators for their contributions.

Data availability statement

Data from this study will be made available to qualified investigators upon reasonable request to the corresponding author.

References

Ahmad, I.M., Temme, J.B., Abdalla, M.Y., Zimmerman, M.C., 2016. Redox status in workers occupationally exposed to long-term low levels of ionizing radiation: A pilot study. Redox Rep. 21, 139–145. https://doi.org/10.1080/13510002.2015.1101891.

Akkaya, B., Roesler, A.S., Miozzo, P., Theall, B.P., Al Souz, J., Smelkinson, M.G., Kabat, J., Traba, J., Sack, M.N., Brzostowski, J.A., Pena, M., Dorward, D.W.,

Pierce, S.K., Akkaya, M., 2018. Increased mitochondrial biogenesis and reactive oxygen species production accompany prolonged CD4. J. Immunol. 201, 3294–3306. https://doi.org/10.4049/jimmunol.1800753.
Ali, S.S., Young, J.W., Wallace, C.K., Gresack, J., Jeste, D.V., Geyer, M.A., Dugan, L.L., Risbrough, V.B., 2011. Initial evidence linking synaptic superoxide production with poor short-term memory in aged mice. Brain Res. 1368, 65–70. https://doi.org/10.1016/j.brainres.2010.11.009.
Ances, B.M., Clifford, D.B., 2008. HIV-associated neurocognitive disorders and the impact of combination antiretroviral therapies. Curr. Neurol. Neurosci. Rep. 8, 455–461.
Ances, B.M., Sisti, D., Vaida, F., Liang, C.L., Leontiev, O., Perthen, J.E., Buxton, R.B., Benson, D., Smith, D.M., Little, S.J., Richman, D.D., Moore, D.J., Ellis, R.J., group, H., 2009. Resting cerebral blood flow: a potential biomarker of the effects of HIV in the brain. Neurology 73, 702–8. 10.1212/WNL.0b013e3181b59a97.
Ances, B.M., Vaida, F., Yeh, M.J., Liang, C.L., Buxton, R.B., Letendre, S., McCutchan, J.A., Ellis, R.J., 2010. HIV infection and aging independently affect brain function as measured by functional magnetic resonance imaging. J. Infect. Dis. 201, 336–340. https://doi.org/10.1086/649899.
Ances, B., Vaida, F., Ellis, R., Buxton, R., 2011. Test-retest stability of calibrated BOLD-fMRI in HIV- and HIV+ subjects. Neuroimage 54, 2156–2162. https://doi.org/10.1016/j.neuroimage.2010.09.081.
Antinori, A., Arendt, G., Becker, J.T., Brew, B.J., Byrd, D.A., Cherner, M., Clifford, D.B., Cinque, P., Epstein, L.G., Goodkin, K., Gisslen, M., Grant, I., Heaton, R.K., Joseph, J., Marder, K., Marra, C.M., McArthur, J.C., Nunn, M., Price, R.W., Pulliam, L., Robertson, K.R., Sacktor, N., Valcour, V., Wojna, V.E., 2007. Updated research nosology for HIV-associated neurocognitive disorders. Neurology 69, 1789–1799. https://doi.org/10.1212/01.WNL.0000287431.88658.8b.
Avdoshina, V., Fields, J.A., Castellano, P., Dedoni, S., Palchik, G., Trejo, M., Adame, A., Rockenstein, E., Eugenin, E., Masliah, E., Mocchetti, I., 2016. The HIV protein gp120 alters mitochondrial dynamics in neurons. Neurotox. Res. 29, 583–593. https://doi.org/10.1007/s12640-016-9608-6.
Becker, J.T., Sanders, J., Madsen, S.K., Ragin, A., Kingsley, L., Maruca, V., Cohen, B., Goodkin, K., Martin, E., Miller, E.N., Sacktor, N., Alger, J.R., Barker, P.B., Saharan, P., Carmichael, O.T., Thompson, P.M., Multicenter AIDS Cohort Study, 2011. Subcortical brain atrophy persists even in HAART-regulated HIV disease. Brain Imag. Behav. 5, 77–85. https://doi.org/10.1007/s11682-011-9113-8.
Buettner, G.R., 2011. Superoxide dismutase in redox biology: the roles of superoxide and hydrogen peroxide. Anticancer Agents Med. Chem. 11, 341–346.
Cadenas, E., Davies, K.J.A., 2000. Mitochondrial free radical generation, oxidative stress, and aging11This article is dedicated to the memory of our dear friend, colleague, and mentor Lars Ernster (1920–1998), in gratitude for all he gave to us. Free Radical Biol. Med. 29, 222–230. https://doi.org/10.1016/S0891-5849(00)00317-8.
Chang, L., Tomasi, D., Yakupov, R., Lozar, C., Arnold, S., Caparelli, E., Ernst, T., 2004. Adaptation of the attention network in human immunodeficiency virus brain injury. Ann. Neurol. 56, 259–272. https://doi.org/10.1002/ana.20190.
Chang, L., Yakupov, R., Nakama, H., Stokes, B., Ernst, T., 2008. Antiretroviral treatment is associated with increased attentional load-dependent brain activation in HIV patients. J. Neuroimmune Pharmacol. 3, 95–104. https://doi.org/10.1007/s11481-007-9092-0.
Cohen, R.A., Harezlak, J., Schifitto, G., Hana, G., Clark, U., Gongvatana, A., Paul, R., Taylor, M., Thompson, P., Alger, J., Brown, M., Zhong, J., Campbell, T., Singer, E., Daar, E., McMahon, D., Tso, Y., Yiannoutsos, C.T., Navia, B., HIV Neuroimaging Consortium, 2010. Effects of nadir CD4 count and duration of human immunodeficiency virus infection on brain volumes in the highly active antiretroviral therapy era. J. NeuroVirol. 16, 25–32. https://doi.org/10.3109/13550280903552420.
Cysique, L.A., Brew, B.J., 2009. Neuropsychological functioning and antiretroviral treatment in HIV/AIDS: a review. Neuropsychol. Rev. 19, 169–185. https://doi.org/10.1007/s11065-009-9092-3.
Efron, B., Tibshirani, R., 1986. Bootstrap methods for standard errors, confidence intervals, and other measures of statistical accuracy. Statist. Sci. 1, 54–75. https://doi.org/10.1214/ss/1177013815.
Elicer, M., I., Byrd, D., Clark, U.S., Morgello, S., Robinson-Papp, J., 2018. Motor function declines over time in human immunodeficiency virus and is associated with cerebrovascular disease, while HIV-associated neurocognitive disorder remains stable. J. Neurovirol. 24, 514–522. 10.1007/s13365-018-0640-6.
Ernst, T., Chang, L., Jovicich, J., Ames, N., Arnold, S., 2002. Abnormal brain activation on functional MRI in cognitively asymptomatic HIV patients. Neurology 59, 1343–1349.
Ernst, T., Yakupov, R., Nakama, H., Crocket, G., Cole, M., Watters, M., Ricardo-Dukelow, M.L., Chang, L., 2009. Declined neural efficiency in cognitively stable human immunodeficiency virus patients. Ann. Neurol. 65, 316–325. https://doi.org/10.1002/ana.21594.
Franchina, D.G., Dostert, C., Brenner, D., 2018. Reactive oxygen species: involvement in T cell signaling and metabolism. Trends Immunol. 39, 489–502. https://doi.org/10.1016/j.it.2018.01.005.
Fritz, M.S., MacKinnon, D.P., 2007. Required sample size to detect the mediated effect. Psychol. Sci. 18, 233–239. https://doi.org/10.1111/j.1467-9280.2007.01882.x.
Fukui, M., Zhu, B.T., 2010. Mitochondrial superoxide dismutase SOD2, but not cytosolic SOD1, plays a critical role in protection against glutamate-induced oxidative stress and cell death in HT22 neuronal cells. Free Radic. Biol. Med. 48, 821–830. https://doi.org/10.1016/j.freeradbiomed.2009.12.024.
Gil, L., Martínez, G., González, I., Tarinas, A., Alvarez, A., Giuliani, A., Molina, R., Tápanes, R., Pérez, J., León, O.S., 2003. Contribution to characterization of oxidative stress in HIV/AIDS patients. Pharmacol. Res. 47, 217–224. https://doi.org/10.1016/s1043-6618(02)00320-1.
González-Casacuberta, I., Juárez-Flores, D.L., Morén, C., Garrabou, G., 2019. Bioenergetics and autophagic imbalance in patients-derived cell models of Parkinson disease supports systemic dysfunction in neurodegeneration. Front. Neurosci. 13 https://doi.org/10.3389/fnins.2019.00894.
Grent-'t-Jong, T., Oostenveld, R., Jensen, O., Medendorp, W.P., Praamstra, P., 2013. Oscillatory dynamics of response competition in human sensorimotor cortex. Neuroimage 83, 27–34. 10.1016/j.neuroimage.2013.06.051.
Grent-'t-Jong, T., Oostenveld, R., Jensen, O., Medendorp, W.P., Praamstra, P., 2014. Competitive interactions in sensorimotor cortex: oscillations express separation between alternative movement targets. J. Neurophysiol. 112, 224–32. 10.1152/jn.00127.2014.
Gross, J., Kujala, J., Hamalainen, M., Timmermann, L., Schnitzler, A., Salmelin, R., 2001. Dynamic imaging of coherent sources: studying neural interactions in the human brain. Proc. Natl. Acad. Sci. U.S.A. 98, 694–699. https://doi.org/10.1073/pnas.98.2.694.
Hara, Y., Yuk, F., Puri, R., Janssen, W.G., Rapp, P.R., Morrison, J.H., 2014. Presynaptic mitochondrial morphology in monkey prefrontal cortex correlates with working memory and is improved with estrogen treatment. Proc. Natl. Acad. Sci. U.S.A. 111, 486–491. https://doi.org/10.1073/pnas.1311310110.
Heaton, R.K., Clifford, D.B., Franklin, D.R., Woods, S.P., Ake, C., Vaida, F., Ellis, R.J., Letendre, S.L., Marcotte, T.D., Atkinson, J.H., Rivera-Mindt, M., Vigil, O.R., Taylor, M.J., Collier, A.C., Marra, C.M., Gelman, B.B., McArthur, J.C., Morgello, S., Simpson, D.M., McCutchan, J.A., Abramson, I., Gamst, A., Fennema-Notestine, C., Jernigan, T. L., Wong, J., Grant, I., Group, C., 2010. HIV-associated neurocognitive disorders persist in the era of potent antiretroviral therapy: CHARTER Study. Neurology 75, 2087–96. 10.1212/WNL.0b013e318200d727.
Heaton, R.K., Franklin, D.R., Ellis, R.J., McCutchan, J.A., Letendre, S.L., Leblanc, S., Corkran, S.H., Duarte, N.A., Clifford, D.B., Woods, S.P., Collier, A.C., Marra, C.M., Morgello, S., Mindt, M.R., Taylor, M.J., Marcotte, T.D., Atkinson, J.H., Wolfson, T., Gelman, B.B., McArthur, J.C., Simpson, D.M., Abramson, I., Gamst, A., Fennema-Notestine, C., Jernigan, T.L., Wong, J., Grant, I., Group, C., Group, H., 2011. HIV-associated neurocognitive disorders before and during the era of combination antiretroviral therapy: differences in rates, nature, and predictors. J. Neurovirol. 17, 3–16. 10.1007/s13365-010-0006-1.
Heinrichs-Graham, E., Arpin, D.J., Wilson, T.W., 2016. Cue-related temporal factors modulate movement-related beta oscillatory activity in the human motor circuit. J. Cogn. Neurosci. 28, 1039–1051. https://doi.org/10.1162/jocn_a_00948.
Heinrichs-Graham, E., McDermott, T.J., Mills, M.S., Wiesman, A.I., Wang, Y.P., Stephen, J.M., Calhoun, V.D., Wilson, T.W., 2018b. The lifespan trajectory of neural oscillatory activity in the motor system. Dev. Cogn. Neurosci. 30, 159–168. https://doi.org/10.1016/j.dcn.2018.02.013.
Heinrichs-Graham, E., Hoburg, J.M., Wilson, T.W., 2018a. The peak frequency of motor-related gamma oscillations is modulated by response competition. NeuroImage 165, 27–34. https://doi.org/10.1016/j.neuroimage.2017.09.059.
Heinrichs-Graham, E., Wilson, T.W., 2015. Coding complexity in the human motor circuit. Hum. Brain Mapp. 36, 5155–5167. https://doi.org/10.1002/hbm.23000.
Heinrichs-Graham, E., Wilson, T.W., 2016. Is an absolute level of cortical beta suppression required for proper movement? Magnetoencephalographic evidence from healthy aging. Neuroimage 134, 514–521. https://doi.org/10.1016/j.neuroimage.2016.04.032.
Heinrichs-Graham, E., Taylor, B.K., Wang, Y.-P., Stephen, J.M., Calhoun, V.D., Wilson, T. W., 2020. Parietal oscillatory dynamics mediate developmental improvement in motor performance. Cereb. Cortex 30, 6405–6414. https://doi.org/10.1093/cercor/bhaa199.
Hillebrand, A., Singh, K.D., Holliday, I.E., Furlong, P.L., Barnes, G.R., 2005. A new approach to neuroimaging with magnetoencephalography. Hum. Brain Mapp 25, 199–211. https://doi.org/10.1002/hbm.20102.
Hohle, R.H., 1965. Inferred components of reaction times as functions of foreperiod duration. J. Exp. Psychol. 69, 382–386. https://doi.org/10.1037/h0021740.
Johnson, F., Giulivi, C., 2005. Superoxide dismutases and their impact upon human health. Mol. Aspects Med., Trace Elements Human Health 26, 340–352. https://doi.org/10.1016/j.mam.2005.07.006.
Kaiser, J., Birbaumer, N., Lutzenberger, W., 2001. Event-related beta desynchronization indicates timing of response selection in a delayed-response paradigm in humans. Neurosci. Lett. 312, 149–152. https://doi.org/10.1016/s0304-3940(01)02217-0.
Kamkwalala, A., Newhouse, P., 2017. Mechanisms of cognitive aging in the HIV-positive adult. Curr. Behav. Neurosci. Rep. 4, 188–197. https://doi.org/10.1007/s40473-017-0122-9.
Kann, O., Kovács, R., 2007. Mitochondria and neuronal activity. Am. J. Physiol.-Cell Physiol. 292, C641–C657. 10.1152/ajpcell.00222.2006.
Korencak, M., Byrne, M., Richter, E., Schultz, B.T., Juszczak, P., Ake, J.A., Ganesan, A., Okulicz, J.F., Robb, M.L., de Los Reyes, B., Winning, S., Fandrey, J., Burgess, T.H., Esser, S., Michael, N.L., Agan, B.K., Streeck, H., 2019. Effect of HIV infection and antiretroviral therapy on immune cellular functions. JCI Insight 4. https://doi.org/10.1172/jci.insight.126675.
Kovach, C.K., Gander, P.E., 2016. The demodulated band transform. J. Neurosci. Methods 261, 135–154. https://doi.org/10.1016/j.jneumeth.2015.12.004.
Lambeth, J.D., 2004. NOX enzymes and the biology of reactive oxygen. Nat. Rev. Immunol. 4, 181–189. https://doi.org/10.1038/nri1312.
Mimiaga, M.J., Reisner, S.L., Grasso, C., Crane, H.M., Safren, S.A., Kitahata, M.M., Schumacher, J.E., Mathews, W.C., Mayer, K.H., 2013. Substance use among HIV-infected patients engaged in primary care in the united states: findings from the centers for AIDS research network of integrated clinical systems cohort. Am. J. Public Health 103, 1457–1467. https://doi.org/10.2105/AJPH.2012.301162.
Nomenclature and research case definitions for neurologic manifestations of human immunodeficiency virus-type 1 (HIV-1) infection. Report of a Working Group of the

American Academy of Neurology AIDS Task Force, 1991. Neurology 41, 778–785. 10.1212/wnl.41.6.778.
Pace, G.W., Leaf, C.D., 1995. The role of oxidative stress in HIV disease. Free Radic. Biol. Med. 19, 523–528. https://doi.org/10.1016/0891-5849(95)00047-2.
Praamstra, P., Kourtis, D., Nazarpour, K., 2009. Simultaneous preparation of multiple potential movements: opposing effects of spatial proximity mediated by premotor and parietal cortex. J. Neurophysiol. 102, 2084–2095. https://doi.org/10.1152/jn.00413.2009.
Rabkin, J.G., 2008. HIV and depression: 2008 review and update. Curr. HIV/AIDS Rep. 5, 163–171. https://doi.org/10.1007/s11904-008-0025-1.
Reaume, Andrew, G., Elliott, J.L., Hoffman, E.K., Kowall, N.W., Ferrante, R.J., Siwek, D. R., Wilcox, H.M., Flood, D.G., Beal, M.F., Brown, R.H., Scott, R.W., Snider, W.D., 1996. Motor neurons in Cu/Zn superoxide dismutase-deficient mice develop normally but exhibit enhanced cell death after axonal injury. Nat. Genet. 13, 43–47. 10.1038/ng0596-43.
Repetto, M., Reides, C., Gomez Carretero, M.L., Costa, M., Griemberg, G., Llesuy, S., 1996. Oxidative stress in blood of HIV infected patients. Clin. Chim. Acta 255, 107–117. https://doi.org/10.1016/0009-8981(96)06394-2.
Robertson, K.R., Smurzynski, M., Parsons, T.D., Wu, K., Bosch, R.J., Wu, J., McArthur, J. C., Collier, A.C., Evans, S.R., Ellis, R.J., 2007. The prevalence and incidence of neurocognitive impairment in the HAART era. AIDS 21, 1915–1921. https://doi.org/10.1097/QAD.0b013e32828e4e27.
Robinson-Papp, J., Gensler, G., Navis, A., Sherman, S., Ellis, R.J., Gelman, B.B., Kolson, D.L., Letendre, S.L., Singer, E.J., Valdes-Sueiras, M., Morgello, S., for the National NeuroAIDS Tissue Consortium, 2020. Characteristics of motor dysfunction in longstanding human immunodeficiency virus. Clin. Infect. Dis. 71, 1532–1538. https://doi.org/10.1093/cid/ciz986.
Samuel, M., Ceballos-Baumann, A.O., Blin, J., Uema, T., Boecker, H., Passingham, R.E., Brooks, D.J., 1997. Evidence for lateral premotor and parietal overactivity in Parkinson's disease during sequential and bimanual movements. A PET study. Brain 120, 963–976. https://doi.org/10.1093/brain/120.6.963.
Saylor, D., Dickens, A., Sacktor, N., Haughey, N., Slusher, B., Pletnikov, M., Mankowski, J., Brown, A., Volsky, D., McArthur, J., 2016. HIV-associated neurocognitive disorder — pathogenesis and prospects for treatment. Nat. Rev. Neurol. 12, 15.
Sena, L.A., Li, S., Jairaman, A., Prakriya, M., Ezponda, T., Hildeman, D.A., Wang, C.R., Schumacker, P.T., Licht, J.D., Perlman, H., Bryce, P.J., Chandel, N.S., 2013. Mitochondria are required for antigen-specific T cell activation through reactive oxygen species signaling. Immunity 38, 225–236. https://doi.org/10.1016/j.immuni.2012.10.020.
Shah, A., Kumar, A., 2016. HIV-1 gp120-mediated mitochondrial dysfunction and HIV-associated neurological disorders. Neurotox. Res. 30, 135–137. https://doi.org/10.1007/s12640-016-9619-3.
Simioni, S., Cavassini, M., Annoni, J.M., Rimbault Abraham, A., Bourquin, I., Schiffer, V., Calmy, A., Chave, J.P., Giacobini, E., Hirschel, B., Du Pasquier, R.A., 2010. Cognitive dysfunction in HIV patients despite long-standing suppression of viremia. AIDS 24, 1243–1250. https://doi.org/10.1097/QAD.0b013e3283354a7b.
Sims-Robinson, C., Hur, J., Hayes, J.M., Dauch, J.R., Keller, P.J., Brooks, S.V., Feldman, E.L., 2013. The role of oxidative stress in nervous system aging. PLoS ONE 8, e68011.
Spooner, R.K., Taylor, B.K., L'Heureux, E., Schantell, M., Arif, Y., May, P.E., Morsey, B., Wang, T., Ideker, T., Fox, H.S., Wilson, T.W., 2021c. Stress-induced aberrations in sensory processing predict worse cognitive outcomes in healthy aging adults. Aging 13. 10.18632/aging.203433.
Spooner, R.K., Wiesman, A.I., O'Neill, J., Schantell, M.D., Fox, H.S., Swindells, S., Wilson, T.W., 2020a. Prefrontal gating of sensory input differentiates cognitively impaired and unimpaired aging adults with HIV. Brain Commun. 2, fcaa080. https://doi.org/10.1093/braincomms/fcaa080.
Spooner, R.K., Wiesman, A.I., Proskovec, A.L., Heinrichs-Graham, E., Wilson, T.W., 2020b. Prefrontal theta modulates sensorimotor gamma networks during the reorienting of attention. Hum. Brain Mapp. 41, 520–529. https://doi.org/10.1002/hbm.24819.
Spooner, R.K., Arif, Y., Taylor, B.K., Wilson, T.W., 2021a. Movement-related gamma synchrony differentially predicts behavior in the presence of visual interference across the lifespan. Cereb. Cortex. https://doi.org/10.1093/cercor/bhab141.
Spooner, R.K., Taylor, B.K., Ahmad, I.M., Dyball, K.N., Emanuel, K., Fox, H.S., Stauch, K. L., Zimmerman, M.C., Wilson, T.W., 2021b. Neural oscillatory activity serving sensorimotor control is predicted by superoxide-sensitive mitochondrial redox environments. PNAS 118. https://doi.org/10.1073/pnas.2104569118.
Spooner, R.K., Taylor, B.K., Moshfegh, C.M., Ahmad, I.M., Dyball, K.N., Emanuel, K., Schlichte, S.L., Schantell, M., May, P.E., O'Neill, J., Kubat, M., Bares, S.H., Swindells, S., Fox, H.S., Stauch, K.L., Wilson, T.W., Case, A.J., Zimmerman, M.C., 2021d. Neuroinflammatory profiles regulated by the redox environment predicted cognitive dysfunction in people living with HIV: A cross-sectional study. EBioMedicine 70, 103487. https://doi.org/10.1016/j.ebiom.2021.103487.
Sun, T., Qiao, H., Pan, P.Y., Chen, Y., Sheng, Z.H., 2013. Motile axonal mitochondria contribute to the variability of presynaptic strength. Cell Rep 4, 413–419. https://doi.org/10.1016/j.celrep.2013.06.040.
Taulu, S., Simola, J., 2006. Spatiotemporal signal space separation method for rejecting nearby interference in MEG measurements. Phys. Med. Biol. 51, 1759–1768. https://doi.org/10.1088/0031-9155/51/7/008.
Thompson, P.M., Dutton, R.A., Hayashi, K.M., Toga, A.W., Lopez, O.L., Aizenstein, H.J., Becker, J.T., 2005. Thinning of the cerebral cortex visualized in HIV/AIDS reflects CD4+ T lymphocyte decline. PNAS 102, 15647–15652. https://doi.org/10.1073/pnas.0502548102.
Tzagarakis, C., Ince, N.F., Leuthold, A.C., Pellizzer, G., 2010. Beta-band activity during motor planning reflects response uncertainty. J. Neurosci. 30, 11270–11277. https://doi.org/10.1523/JNEUROSCI.6026-09.2010.
Uusitalo, M.A., Ilmoniemi, R.J., 1997. Signal-space projection method for separating MEG or EEG into components. Med. Biol. Eng. Comput. 35, 135–140.
Valcour, V., Watters, M.R., Williams, A.E., Sacktor, N., McMurtray, A., Shikuma, C., 2008. Aging exacerbates extrapyramidal motor signs in the era of highly active antiretroviral therapy. J. NeuroVirol. 14, 362–367. https://doi.org/10.1080/13550280802216494.
van der Windt, G.J., Everts, B., Chang, C.H., Curtis, J.D., Freitas, T.C., Amiel, E., Pearce, E.J., Pearce, E.L., 2012. Mitochondrial respiratory capacity is a critical regulator of CD8+ T cell memory development. Immunity 36, 68–78. https://doi.org/10.1016/j.immuni.2011.12.007.
Vos, M., Lauwers, E., Verstreken, P., 2010. Synaptic mitochondria in synaptic transmission and organization of vesicle pools in health and disease. Front. Synaptic Neurosci. 2 https://doi.org/10.3389/fnsyn.2010.00139.
Wang, X., Foryt, P., Ochs, R., Chung, J.-H., Wu, Y., Parrish, T., Ragin, A.B., 2011. Abnormalities in resting-state functional connectivity in early human immunodeficiency virus infection. Brain Connect. 1, 207–217. https://doi.org/10.1089/brain.2011.0016.
Wang, X., Wang, W., Li, L., Perry, G., Lee, H., Zhu, X., 2014. Oxidative stress and mitochondrial dysfunction in Alzheimer's disease. Biochim. Biophys. Acta (BBA) 1842, 1240–1247. https://doi.org/10.1016/j.bbadis.2013.10.015.
Wiesman, A.I., Koshy, S.M., Heinrichs-Graham, E., Wilson, T.W., 2020. Beta and gamma oscillations index cognitive interference effects across a distributed motor network. Neuroimage. https://doi.org/10.1016/j.neuroimage.2020.116747, 116747.
Wilkins, J.W., D, P., Robertson, K.R., D, P., Snyder, C.R., n.d. Implications of self-reported cognitive and motor dysfunction inHIV-positive patients.
Wilson, T.W., Heinrichs-Graham, E., Robertson, K.R., Sandkovsky, U., O'Neill, J., Knott, N.L., Fox, H.S., Swindells, S., 2013. Functional brain abnormalities during finger-tapping in HIV-infected older adults: a magnetoencephalography study. J. Neuroimm. Pharmacol. 8, 965–974. https://doi.org/10.1007/s11481-013-9477-1.
Wilson, T.W., Heinrichs-Graham, E., Becker, K.M., 2014. Circadian modulation of motor-related beta oscillatory responses. Neuroimage 102 (Pt 2), 531–539. https://doi.org/10.1016/j.neuroimage.2014.08.013.
Yokoi, A., Diedrichsen, J., 2019. Neural organization of hierarchical motor sequence representations in the human neocortex. Neuron 103, 1178–1190.e7. https://doi.org/10.1016/j.neuron.2019.06.017.
Zhou, Y., Li, R., Wang, X., Miao, H., Wei, Y., Ali, R., Qiu, B., Li, H., 2017. Motor-related brain abnormalities in HIV-infected patients: a multimodal MRI study. Neuroradiology 59, 1133–1142. https://doi.org/10.1007/s00234-017-1912-1.